AIAA JOURNAL
Vol. 38, No. 12, December 2000

Simulation of Deployment Dynamics of Inflatable Structures

Moktar Salama,* C. P. Kuo,† and Michael Lou*
Jet Propulsion Laboratory, California Institute of Technology, Pasadena, California 91109

Analytical simulation of the inflation process of inflatable structures is key to assessing their robust deployment in a space environment. Although the problem seems to be intractable, a simplified finite volume inflation model is developed, which allows discretized description of the gas flow, pressure variation, and resulting nonlinear large deformation throughout domains of the inflatable structure. Simulation results are presented along with convergence studies, which provide insight into the deployment of three different packaging/deployment schemes: Z-unfolding, rollout, and extrusion of a cylindrical tube. The proposed inflation model is not limited to prismatic one-dimensional components and can be applied to inflatable shapes with complex configurations. As a validation of the numerical simulation, a laboratory experiment was conducted on the Z-folded configuration. Generally, good agreement in the overall inflation dynamics is observed between the analysis and experiment.

I. Introduction

SEVERAL space missions have considered the use of lightweight inflatable structures for components such as booms, sunshades, solar concentrators, solar sails, and antennas for nearly all aspects of Earth and space explorations. As a prelude to these missions, the inflatable antenna experiment (IAE) was deployed from the Space Shuttle *Endeavour* in May 1996 to demonstrate the readiness and reliability of the inflatable technology for a large 14-m antenna structure in a realistic space environment.[1] One of the urgent technology issues revealed by the brief 80-min IAE flight experiment was the need to better understand the dynamics of deploying inflatable structures in space and how the inflation process is influenced by the deployment scheme. This includes the initial packaging and subsequent release and inflation. Depending on the deployment scheme, large inflatable structures can be extremely flexible to the point of instability, especially during the early stages of inflation. Rigidization can begin only after final deployment is achieved. Testing the deployment of a large inflatable in an Earth environment in the presence of gravity and air is of limited value for inferring its deployment behavior in space. Therefore, analytical models for simulating and predicting the dynamics of the inflation process are essential tools for understanding inflatables' deployment behavior in space environment and for guiding and improving future packaging and deployment concepts.

To this end, this paper explores the use of a finite volume inflation model that allows a tractable simulation of the deployment process of various inflatable configurations, from their initial stowed state to full deployment. Of interest here is a description of all states of inflation as a function of time. Knowledge of all states of inflation is essential for subsequent assessment of conditions of stability and controllability of the deployment process.

II. Deployment Concepts

Deployment schemes that have been proposed for inflatable structures may be classified dynamically as unrestricted free deployment and controlled or guided deployment.[2] This classification is closely related to details of the initial packaging and the mechanisms used during inflation to control the release of the inflated and yet to be inflated segments of the structure.

In the unrestricted deployment, inflated or partially inflated segments of the structure are not restrained from moving freely in space once released. In the process, their inertia could drag along other uninflated segments, thereby giving rise to the deployment of components with an undesirably high degree of flexibility. As a result, the system may become unstable before achieving full inflation. In controlled deployment, however, only inflated segments of the structure are allowed to deploy in space. Because fully inflated segments have much higher stiffness than partially inflated segments, systems with controlled deployment will tend to be much more stable dynamically.

The Z-folded packaging of tubes and lenticular membranes used in the IAE experiment is an example of unrestricted deployment. On the other hand, the so-called mandrel-guided extrusion (Sec. IV) is an example of controlled deployment. The mandrel extrusion, however, can be used only for inflating structural components having prismatic shapes such as one-dimensional tubes and is not applicable for other general shapes such as a torus or components of lenticular forms. Another example of controlled deployment has been used for the inflatable space synthetic aperture radar,[3] in which the inflatable structure is initially packaged by rolling. The latter scheme is perhaps the most common of the three concepts cited here. Depending on the configuration, rolling can be in a single or in multiple directions. In addition, passive controls of deployment can be introduced, typically in the form of built-in resistive force elements such as coil springs or surface-mounted Velcro strips. Thus, control of the deployment can be achieved at the expense of extra mass and complexity, which, if excessive, could outweigh the advantages of inflatables over their traditional mechanical counterparts. Here, too, a tractable analysis tool can help select the most attractive design alternatives.

In the following, we develop an inflation modeling approach, then apply it to simulating the three aforementioned deployment concepts for inflatable prismatic cylindrical tubes.

III. Inflation Model

The forces that activate the deployment of inflatable membrane structures are dominated by interactions between the internal pressure variation generated by the flow of the inflating gas and the flexible membrane that forms the inflatable enclosure. When modeling this interaction, it is important to capture the correct spatial and temporal variation of the gas pressure $P(x, y, z, t)$ on the inflatable membrane. This is accomplished here by employing an idealization analogous to the finite element disctretization of solids. As shown in Fig. 1, the continuum of enclosed volume is discretized in its stowed state into a set of connected smaller enclosures or finite volumes, or compartments. Continuity of the flow between these finite volumes is provided mathematically by artificial common baffles that vent to each other through artificial orifices. Starting with the stowed state as the initial condition, the inflating gas enters the first finite volume and, in turn, flows to other contiguous volumes through the artificial orifices. Among other variables, the amount of flow between typical finite volumes m and n is a function of the orifice area A_{mn}, the

Presented as Paper 99-1521 at the AIAA/ASME/ASCE/AHS/ASC 40th Structures, Structural Dynamics, and Materials Conference, St. Louis, MO, 12–15 April 1999; received 13 May 1999; revision received 10 June 2000; accepted for publication 19 June 2000.

*Principal Staff, Applied Mechanics. Associate Fellow AIAA.
†Senior Staff, Applied Mechanics. Senior Member AIAA.

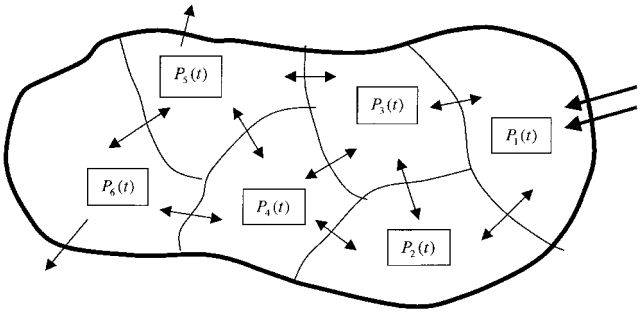

Fig. 1 Discretization of inflatable enclosure into connected finite volumes.

magnitude of which is allowed to vary in proportion to the local area of the associated baffle. In the initial stowed state, all orifices are given infinitesimally small areas. As inflation progresses, these areas are gradually increased to equal the local inflated baffle areas at full inflation. If there are folds in the stowed configuration, it is expedient to locate some of the artificial baffles/orifices at the fold lines because fold lines provide natural constriction of the flow. If there are no fold lines, discretization of the enclosed volume and location of the baffles can be chosen judiciously to emulate the actual flow. Leakage to the outside, if present, can be modeled similarly by venting the finite volume(s) in question to the open external volume.

The forgoing spatial discretization of the gas flow permits a tractable computation of the instantaneous pressure $P_m(t)$ for all discrete volumes m as function of time. As inflation progresses, the computed pressure values are applied to the membrane walls enclosing the inflatable finite volume. The walls themselves can be modeled as thin-walled shells, either analytically in closed form or by the usual finite element technique. Consistency between the finite element and finite volume models should be maintained, at least geometrically, but the degree of element refinement does not need be the same.

Consider an ideal gas flowing between two finite volumes m and n, across orifice A_{mn}. Depending on the ratio of pressures downstream and upstream from the orifice, the gas flow may be subsonic or sonic. For subsonic flow, the rate of flow $\mathrm{d}m_{mn}$ of mass of gas across the orifice can be approximated by a one-dimensional quasi-steady flow,[4] here expressed by

$$\frac{\mathrm{d}m_{mn}}{\mathrm{d}t} = kA_{mn}P_d\left\{\left(\frac{1}{GT}\right)\left(\frac{2\gamma}{\gamma-1}\right)\times\left(\frac{P_o}{P_d}\right)^{(\gamma-1)/\gamma}\times\left[\left(\frac{P_u}{P_d}\right)^{(\gamma-1)/\gamma}-1\right]\right\}^{\frac{1}{2}} \tag{1}$$

where P_o, P_u, and P_d are, respectively, the initial pressure, upstream pressure, and downstream pressure, γ is the specific heat ratio, G is the gas constant, T is the gas temperature, and k is the orifice coefficient.[5]

Similarly, when the flow is sonic, it can be approximated in one dimension by

$$\frac{\mathrm{d}m_{mn}}{\mathrm{d}t} = kA_{mn}P_d\left[\left(\frac{1}{GT}\right)\left(\frac{2\gamma}{\gamma+1}\right)^{(\gamma+1)/(\gamma-1)}\times\left(\frac{P_u}{P_d}\right)^{(\gamma+1)/\gamma}\right]^{\frac{1}{2}} \tag{2}$$

Depending on the type and direction of flow, either of the nonlinear equations (1) or (2) can be integrated numerically for each pair of volumes m and n to calculate the mass of gas $\Delta m(t)$ transferred between them at each discrete time t in the simulation. If one assumes that the density is constant, the corresponding change in volume of each finite volume, for example, m, due to gas flow can be computed as $[\Delta V_f(t)]_m$. Other volumetric changes, here collectively referred to as $[\Delta V_v(t)]_m$, arise from large deformations of the membrane shell itself, partly due to flexibility of the skin or due to contact forces between the inflated surfaces or any other source of deformation. The total change in volume of finite volume m is simply the sum of all aforementioned effects:

$$\Delta V_m(t) = [\Delta V_f(t) + \Delta V_v(t)]_m \tag{3}$$

The corresponding updated pressure is then found for a typical finite volume from

$$P_m(t) = P_o\{V_o/[V_o - \Delta V_m(t)]\}^{\gamma} \tag{4}$$

For a given distribution of pressures $P_m(t)$, $m = 1, \ldots, N$ applied to all N discrete volumes of the inflatable structure, one can propagate computation of the deformations dynamically to the next time step in the simulation. A gas flow model that employs Eqs. (1–4) was successfully employed in simulating attenuation in the airbag impact dynamics during Mars landing.[6] Other applications have also used similar concepts.[7]

IV. Numerical Simulations

In this section, simulation results are presented for the inflation of a cylindrical tube, initially stowed in three different configurations. Two different types of nonlinear dynamics software were selected for model implementation: LS-DYNA3D (Ref. 8) and ADAMS (Ref. 9). Both of these are commercially available, nonlinear, large deformation, dynamic analysis software tools, but each employs different computational primitives and environments.

A. Deployment of Z-Folded Tube

Consider the inflation of a cylindrical tube (diameter of 7 cm, length of 20 cm, 0.0125 cm thick, $E = 18E + 10$ N/m^2), initially folded flat into two overlapping segments. A finite element model of the flexible tube walls in its folded state was constructed in a free–free condition, as shown in the lower left corner of Fig. 2. Over 900 shell elements capable of membrane and bending behavior were used. The folded tube enclosure was also modeled by two finite volumes separated by an artificial baffle and orifice at the fold line. Clearly, discretization of this two-fold inflatable tube into only two finite volumes is a minimum for first-order accuracy of describing the spatial pressure variation during deployment. The inflating gas is introduced mathematically into the first volume in the form of mass flow rate as a function of time. The gas then flows to the second finite volume across the orifice, whose area is proportional to the cross-sectional area of the baffle at the fold.

The presence of contact between surfaces of the tube is monitored during inflation using the so-called surface contact algorithm.[8] In this algorithm, the normal distances between nearest pairs of nodes are checked against a predetermined penetration tolerance. Account is taken of the shell thickness and whether penetration is approaching from the negative or positive side of the surface. If penetration is detected at a pair of nodes, a pair of equal and opposite nodal forces is applied proportional to the penetration distance and surface stiffness k_i. The surface stiffness is approximated by

$$k_i = \left(0.1 \times K_i A_i^2 \big/ V_i\right) \tag{5}$$

where K_i, A_i, and V_i are, respectively, the bulk modulus and the area and volume of the element containing the contacting segment. At nodes in contact, we also apply contact viscous damping ($\sim 10\%$) and coulomb friction having static and dynamic coefficients equal to 0.08 and 0.05, respectively.

The results in Fig. 2 show that the gas flow allows relatively slow pressure buildup into the first volume, along with a gradual opening of the initially constricted cross section at the fold line (artificial orifice). As constriction of the fold erodes, the pressure in the second volume increases to equal the pressure in the first volume, immediately after the second fold snaps open. The maximum pressure differential between the two folds is about 280 N/m^2. For the two-fold configuration considered, one observes a nearly 20% time lag in pressurization between the two folds. This lag is dependent on

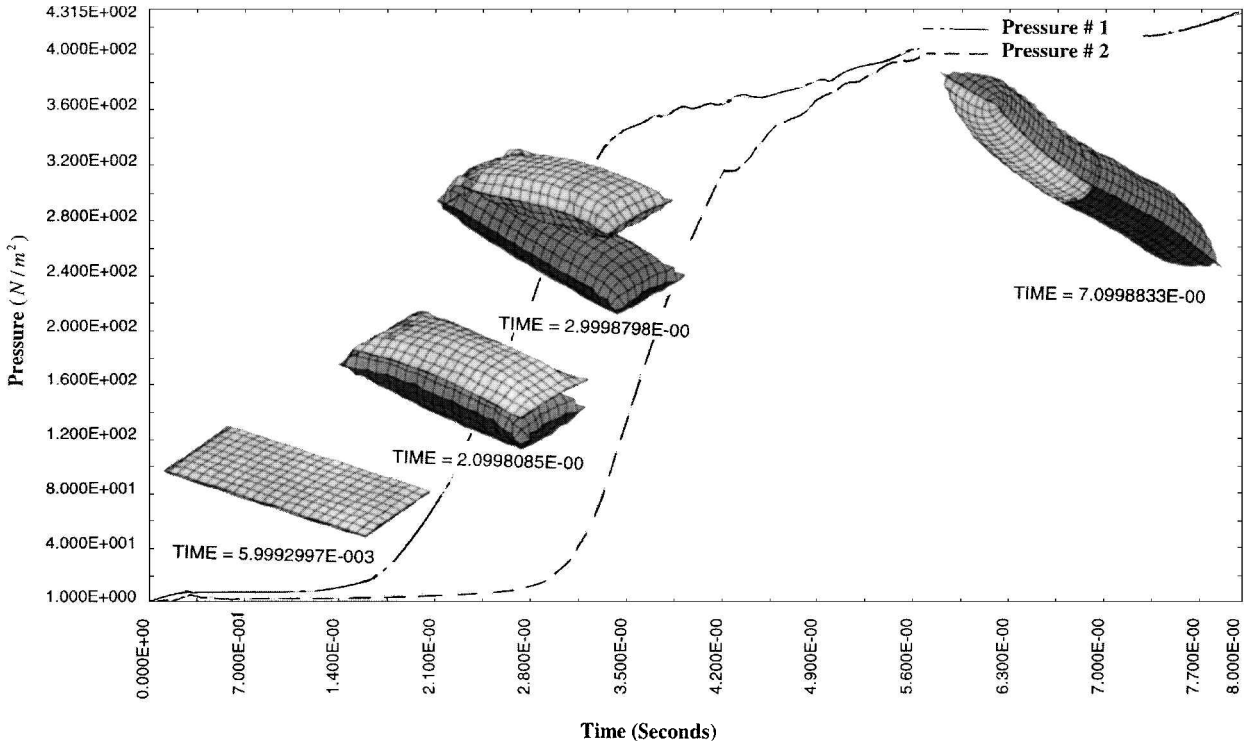

Fig. 2 Deployment of a Z-folded tube.

many parameters, including the shell model, surface contact model, and variation of orifice area with time. In a multiple-fold configuration, the pressurization lag between the first and last fold is expected to increase with the number of folds. The implication here is that multiple Z-fold configurations tend to have a larger percent of the tube length free to deploy while not fully pressurized. This leads to opportunities for dynamic instability, which can be excited by discontinuity in the contact forces. Just before the opening of each fold, the contact forces tend to reach their maximum and then become zero once the fold opens.

B. Rollout Deployment

The circular tube under consideration is 5.6 cm in diameter, is 20 cm long, and is made of 0.0125-cm-thick fabric material. The material properties are assumed to be the same as in the preceding example. Initially, the tube is rolled in the form of an Archimedean linear spiral shape governed by the relationship $r = a\theta$ as in the configuration shown in the lower left corner of Fig. 3. The finite element model of this configuration is free–free and consists of 392 shell elements connecting 364 surface nodes. On the other hand, the finite volume inflation model is invoked by subdividing the stowed tube enclosure into five finite inflatable volumes along the rolling direction, separated by four sets of artificial baffles and orifices. Two of the five volumes are in the straight section of the tube, and the remaining ones are in the spiral section. Contiguous pairs of volumes are allowed to vent to each other across the common artificial orifice. As in the earlier example, the area of each orifice is function of the local cross-sectional area. Initially, all orifice areas are nearly zero, but they increase sequentially and gradually as inflation progresses from one end of the tube to the other.

In terms of contact forces, no scheme of deployment is more dominated by continuity of forces between contacting surfaces than in rollout deployment. In rollout deployment, once the straight part of the tube is inflated, contact surface forces will remain near their peak while marching spatially along the rollout path until complete deployment. This is true as long as the inflation pressure is monotonically maintained. The sequence of deployment and pressure buildup as gas flows from the straight end to the spiral part is shown in Fig. 3. The time at which each of the images was taken from the animation corresponds approximately to the time location on Fig. 3. For example, the last image shown is recorded when the tube was nearly cylindrical but not completely inflated. Further pressure increase to about 1800 N/m^2 was accompanied by elastic stretching of the membrane. A maximum pressure differential of about 180 N/m^2 is observed between the two ends of the tube. Unlike the Z-folded configuration, the stability of deployment of rolled tubes is maintained, not only by the restoring forces in the spiral membrane but also by the relatively smooth variation of the rollout forces between surfaces in contact. In the present results, additional resistive forces (due to a spiral spring or Velcro) were not modeled but will be included in future work.

C. Extrusion Deployment

The following simulation of deployment by mandrel extrusion of a cylindrical tube is performed here within the framework of ADAMS software. Although primitives in ADAMS are best suited for simulating rigid-body dynamics, they provide the ability to model flexible bodies, mostly by functional representation of the forces present. In the inflation deployment by mandrel extrusion, the tube is literally extruded out of the mandrel (in which it was initially stowed) as it is inflated. Although the inflation pressure can vary with time, it is nearly uniform spatially. Therefore, only one finite volume is necessary to model the gas flow here.

Consider the inflation of a tube with diameter of 10 cm, length of 30 cm, and thickness of 0.01 cm. In this case, a one-dimensional flexible model is constructed for the inflatable volume. Here, the state variable is the deployed position $z(t)$ of the closed end of the tube relative to the fixed mandrel. Initially, $z(0) = 0$. Then, the inflating gas is introduced into the mandrel side of the tube through an orifice connection to an inflation canister. At a typical instant of time, the inflating gas creates internal pressure $P_1(t)$ in the tube, the magnitude of which is governed by Eqs. (1–4). The pressure forces $P_1(t)$ are simulated in ADAMS software along with other forces, such as forces due to tube's longitudinal stiffness $= 2\pi r t_0 E \times z/L$, time-dependent mass of the inflated tube, and damping forces proportional to the velocity of inflation. The elastic modulus used in the stiffness expression is approximated by the one-dimensional constitutive relationship of wrinkled membrane in Fig. 4. This constitutive relation is consistent with results suggested by the experiments of Ref. 10.

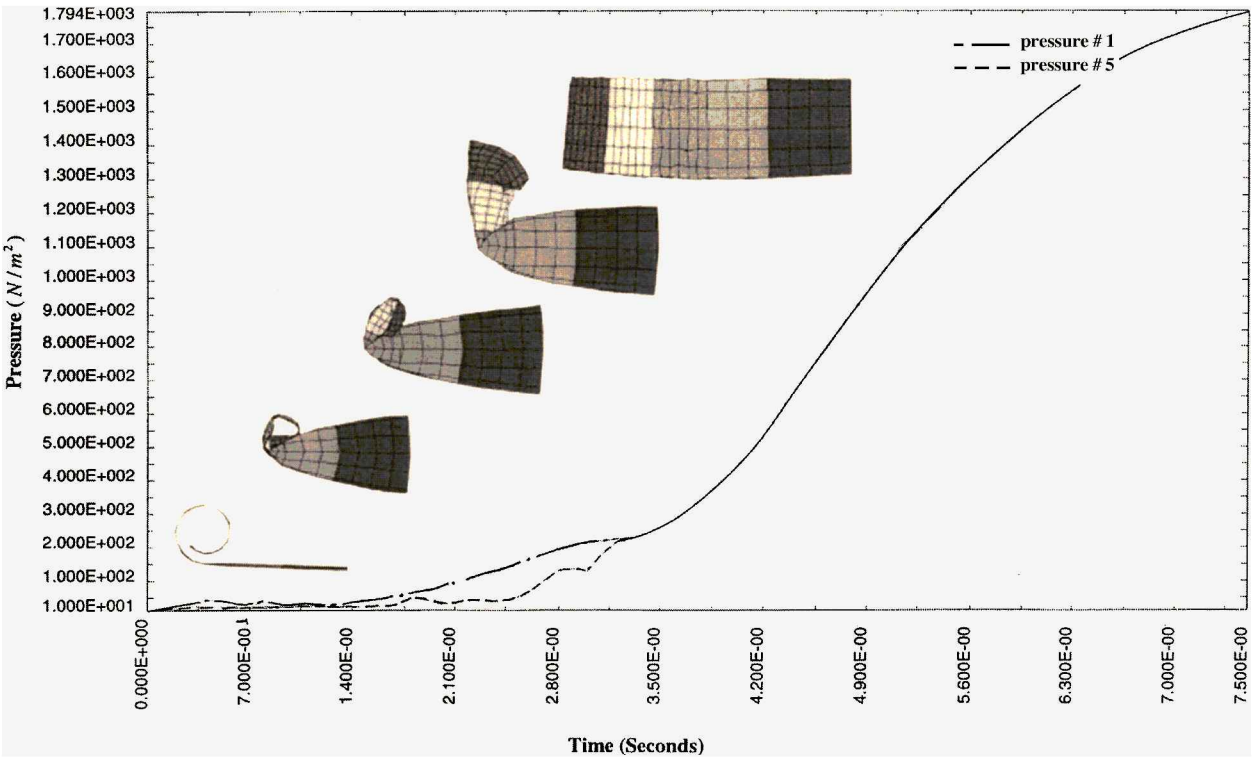

Fig. 3 Deployment of a rollout tube.

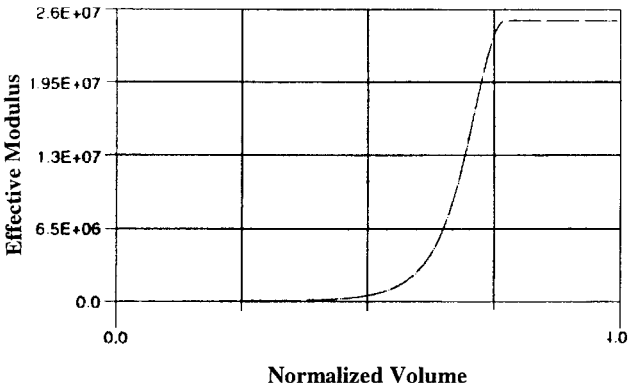

Fig. 4 Constitutive model of wrinkled membrane.

The results of simulation are shown in Fig. 5. As in earlier cases, the pressure internal to the tube is shown as function of time. Here, a small leak (2 mm^2) that vents to the outside is assumed to be active between $t = 1.75$ and 2.0 s. Four images are selected from the animation at different time instances and are superimposed on the pressure curve in Fig. 5. Whereas full pressurization is reached at about 3 s, full inflation was not achieved until after approximately 4 s.

V. Numerical Convergence

The simplified modeling approach introduced in this paper has been prompted by the extreme analytical difficulty of the problem at hand. It is also because of this that one finds it difficult to invoke rigorous proofs of convergence and accuracy of the numerical approximations. However, to give an indication of the nature of expected numerical performance of the proposed scheme, we present the results of convergence studies conducted using the rollout deployment configuration of Sec. IV.B. There are several approximation sources involved in the process. These include sources arising from the usual finite element discretization, involving nonlinear large deformation elasticity with and without contact nonlinearity, as well as sources arising from the approximation of the continuous three-dimensional fluid flow by a discrete one-dimensional finite volume flow.

In the following numerical experiments, emphasis is placed on convergence behavior due to the finite volume flow approximation. This is achieved by varying the number of finite volumes, while keeping all other model parameters unchanged. The pressure distribution history is shown in Figs. 6 and 7 for two cases where, in Fig. 6, a single finite volume occupying the entire rolled tube cavity is used, whereas in Fig. 7, 10 finite volumes are used along the rolling direction to simulate a more refined spatial and temporal progress of inflation. In Fig. 7, each of the 10 pressure curves represents a pressure history (numbered 1–10), with number 1 (top curve) representing the first finite volume through which air enters and the lower curve representing the finite volume at the extreme end of the tube (number 10). All other pressure history curves for intermediate finite volumes do lie in between the 1st and 10th, indicating that volume 1 is the leading one, followed by volumes 2, 3, . . . , 10. As an indication of convergence, note that the pressure curve for Fig. 6a for only one finite volume is bounded by the extreme (top and lower) curves of Fig. 7 using 10 finite volumes.

Numerical experiments for other intermediate cases of discretization, with two and five finite volumes, were also made. Because the significance of the increased number of finite volumes is in increased pressure phase lag/lead between the extreme ends of the tube, we show comparison of the discretization refinement in Fig. 8 as time histories of the differential pressure between the two ends of the tube. Consistent with the physical expectation, Fig. 8 shows increased pressure phasing as the number of finite volumes is increased. Depending on the inflatable configuration, although a highly refined finite element model of the membrane enclosure may be necessary, a relatively coarse finite volume model can be sufficient. However, if only one finite volume is used, the pressure will be invariant inside the entire inflatable cavity, and the resulting inflation sequence will be physically incorrect in that all folds will open simultaneously.

VI. Validation Experiment

As a simple validation of the numerical simulation, a controlled laboratory experiment was conducted using the configuration of Sec. IV.A in which the tube is initially folded flat into two overlapping segments. The same approximate dimensions and material properties apply here. Inflation of the folded tube was provided by a pneumatic air pump fitted with a pressure regulator and flowmeter to

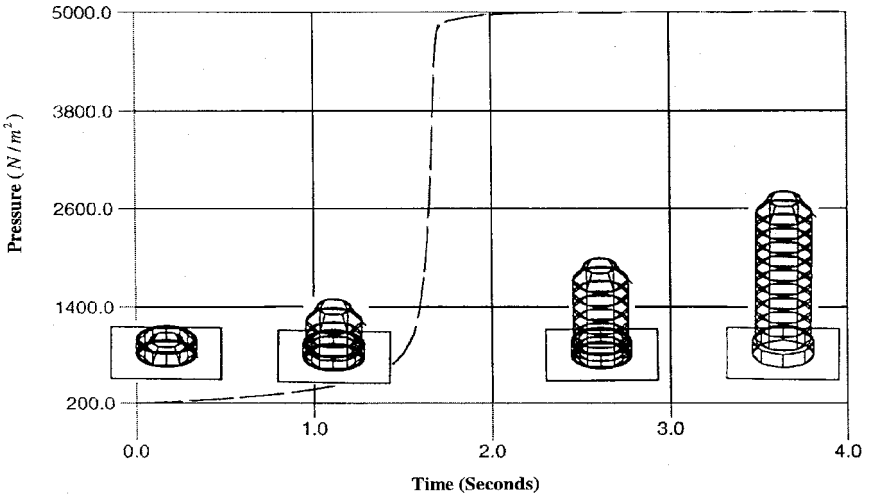

Fig. 5 Deployment of tube by extrusion.

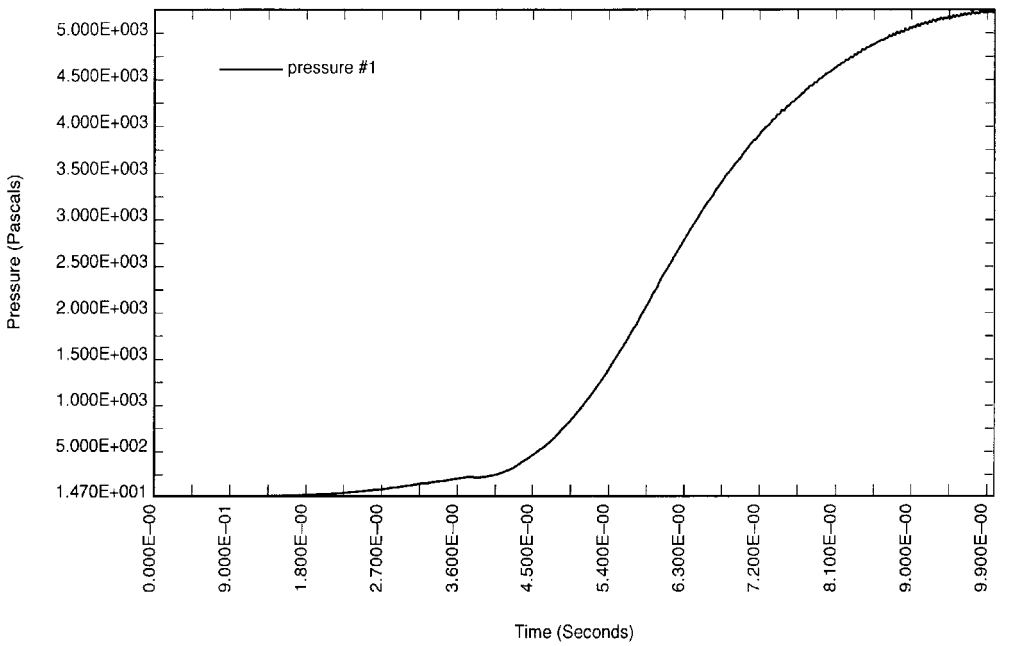

Fig. 6 Pressure distribution in inflatable tube modeled by one finite volume.

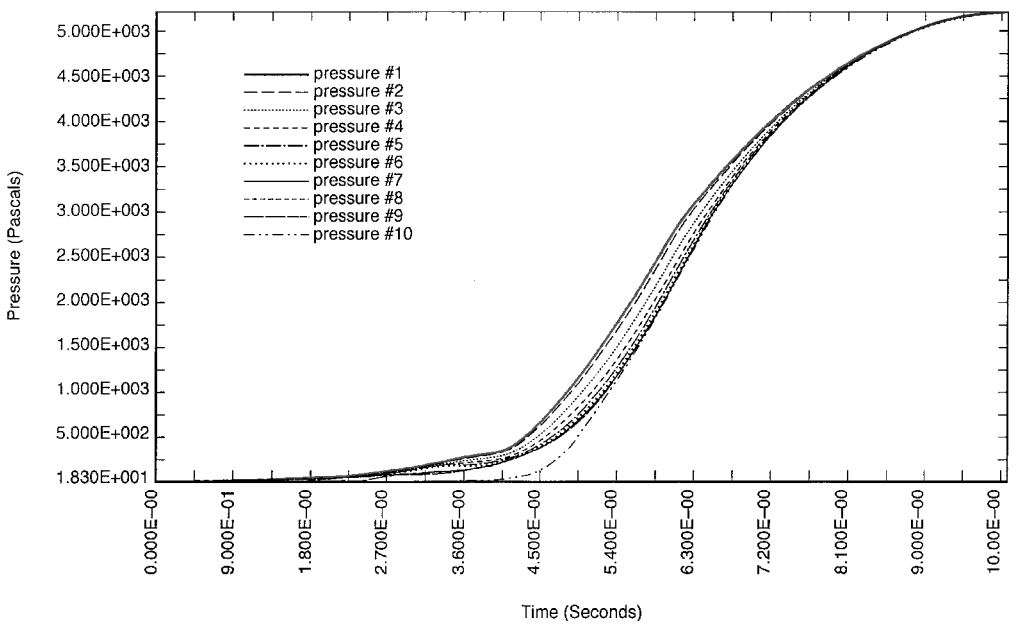

Fig. 7 Pressure distribution in inflatable tube modeled by 10 finite volumes.

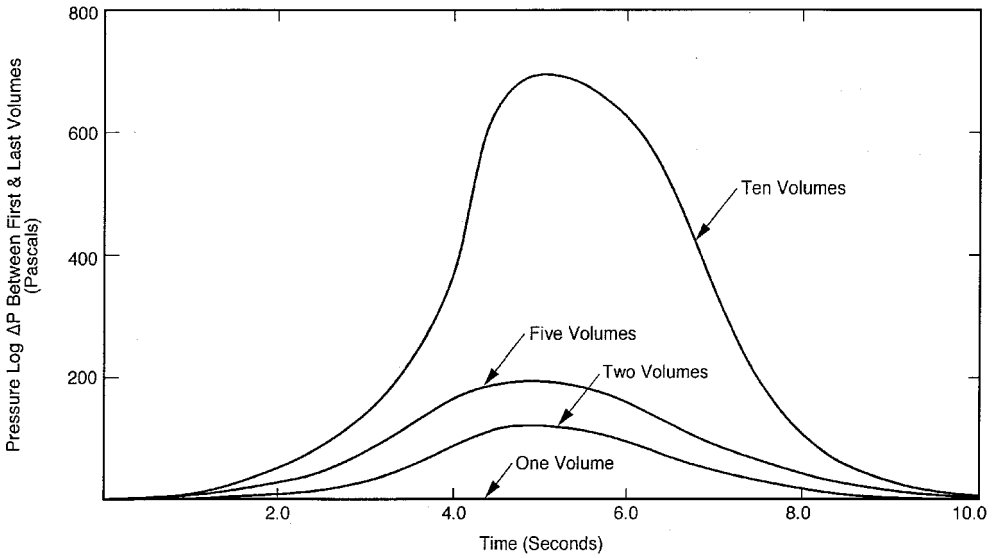

Fig. 8 Maximum pressure difference within tube as function of number of finite volumes.

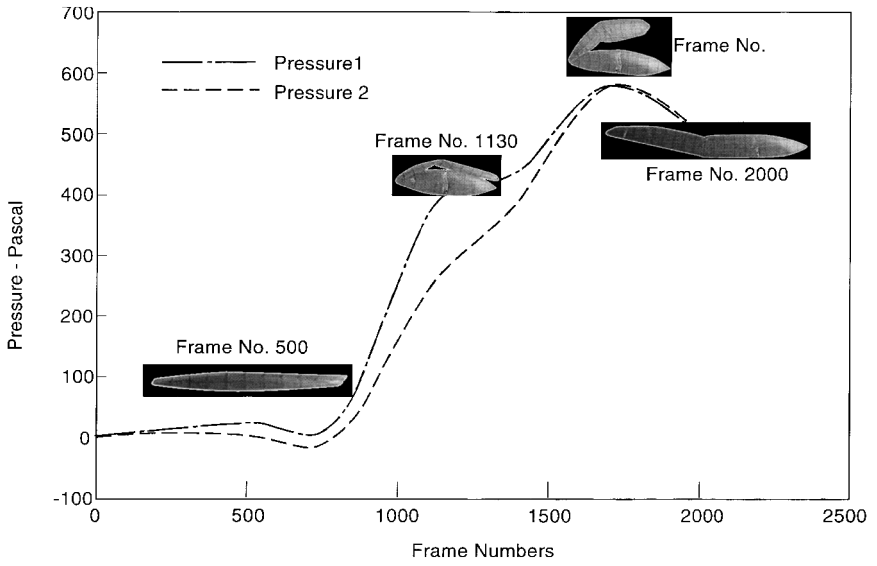

Fig. 9 Experimental deployment of a Z-folded tube.

measure and control the airflow into the tube. The pressure in each of the folds was monitored by separate pressure gauges attached to 1.5-mm silicone tubing inserted halfway inside each fold. A high-resolution digital video camera was used for optical imaging of the inflation experiment. The images were subsequently captured frame by frame into a personal computer using commercially available software for further analysis and data reduction.

In Fig. 9, the results of the experiment are presented in a form analogous to Fig. 2. However, before a comparison is made, we note the differences between conditions of the experiment and analysis. Simplicity of the experimental setup allowed relatively slow inflation of the tube, about 1.5 min compared to the higher rate of few seconds used in the analysis. Slowing down the inflation rate in the analysis would increase the calculation time considerably. Furthermore, both gravity and the internal silicone tubing inserted in the folds to monitor the pressure were not modeled in the analysis. Thus, a comparison between Figs. 2 and 9 can only be made qualitatively, with test time replaced by an imaging frame. Despite these limitations, there is good agreement between the pressurization curves in the experiment and simulation, not only in the variation of pressure in each fold with time, but also in the magnitude of differential pressure between folds. This is also evident from a qualitative comparison of the degree of inflation indicated by images from the experiment and from analysis. The kink in the upper fold of the experiment images, Fig. 9, is due to the additional mass and stiffness of the silicone tube inserted in the upper fold to monitor the pressure.

Considering the aforementioned limitations, it is encouraging to note that the simplified inflation model and analysis approach discussed herein is capable of capturing the overall dynamics of inflation relatively well, in spite of the strong nonlinearity of the problem.

VII. Summary

The primary objective of this paper was to explore the use of analysis simulation as a tool for predicting the dynamic behavior of the deployment process of inflatable structures in space. This is desirable because experimental ground verification of these highly flexible nonlinear structures is often not possible. For this purpose, a finite volume inflation model was developed and successfully employed in simulating the deployment dynamics of inflatable tubes. By discretizing the initial continuum of inflatable enclosure into a set of connected smaller enclosures of finite volumes, one can compute the spatial variation of pressure during inflation throughout the inflatable cavity. The convergence studies indicate that multiple finite volumes must be used in the flow model. If only one finite volume is used, the pressure will be invariant inside the entire inflatable cavity. The resulting inflation sequence will then be physically incorrect in that all folds will open simultaneously.

The three examples selected represented different schemes for inflating prismatic structural components, such as tubes. However, the finite volume inflation model is not limited to prismatic components. In fact, it is most useful for modeling the deployment of inflatable shapes with complex configurations. In spite of the limitations noted with regard to the analysis and experimental conditions, the simulations captured the overall dynamics of deployment relatively well.

Acknowledgments

This research was performed at the Jet Propulsion Laboratory (JPL), California Institute of Technology, under contract with NASA. Funding was provided by the JPL Director's Research and Development Fund and by NASA's Cross Enterprise Technology Development Program. We gratefully acknowledge the help of J. J. Wu, JPL, in the setup of the experiment.

References

[1]Freeland, R. E., and Veal, G. R., "Significance of the Inflatable Antenna Experiment Technology," AIAA Paper 98-2104, April 1998.

[2]Salama, M., Lou, M., and Fang, H., "Deployment of Inflatable Space Structures: A Review of Recent Developments," AIAA Paper 2000-1730, April 2000.

[3]Lou, M. C., Feria, V. A., and Huang, J., "Development of an Inflatable Space Synthetic Aperture Radar," AIAA Paper 98-2103, April 1998.

[4]Van Wylen, G., Sonntag, R., and Borgnakke, C., *Fundamentals of Classical Thermodynamics*, Wiley, New York, 1994.

[5]Perry, J. A., Jr., "Critical Flow Through Sharp Edged Orifices," *Transactions of the American Society of Mechanical Engineers*, Oct. 1949, pp. 757–764.

[6]Salama, M., Davis, G., Kuo, C. P., Rivellini, T., and Sabahi, D., "Simulation of Airbag Impact Dynamics for Mars Landing," AIAA Paper 96-1209, April 1996.

[7]McKinney, J., and Taylor, T., "Use of LS-DYNA3D to Simulate Airbag Landing Impact Attenuation of the Kistler K1 Reusable Launch Vehicle," LS-DYNA Users Conf., Detroit, MI, Sept. 1998.

[8]Hallquist, J. O., *LS-DYNA3D, Theoretical/User's Manual*, Livermore Software Technology Corp., Livermore, CA, 1993.

[9]*Automatic Dynamic Analysis Mechanical Systems (ADAMS)/Solver Reference Manual*, Ver. 9.1, Mechanical Dynamics, Ann Arbor, MI, 1998.

[10]Ruggiero, T. J., and Mikulas, M. M., "A One Dimensional Constitutive Model for Wrinkled Thin Polymer Films," NASA CR 201706, June 1997.

S. K. Aggarwal
Associate Editor